Electronic Supplementary Material (ESI) for Energy & Environmental Science.
This journal is © The Royal Society of Chemistry 2022

Supplementary information for

Durable, stretchable and washable inorganic-based woven thermoelectric textiles for power generation and solid-state cooling

Yuanyuan Zheng[1], Xue Han[1], Jiawei Yang[2, 5], Yuanyuan Jing[1], Xinyi Chen[1], Qianqian Li[1, 6], Ting Zhang[3, 7], Guodong Li[2], Hangtian Zhu[2], Huaizhou Zhao[2], G. Jeffrey Snyder[4], Kun Zhang[1*]*

[1]Key Laboratory of Textile Science & Technology (Ministry of Education), College of Textiles, Donghua University, Shanghai 201620, PR China

[2]Beijing National Laboratory for Condensed Matter Physics, Institute of Physics, Chinese Academy of Sciences, Beijing 100190, PR China

[3]Institute of Engineering Thermophysics, Innovation Academy for Light-duty Gas Turbine, Chinese Academy of Sciences, Beijing 100190, PR China

[4]Department of Materials Science and Engineering, Northwestern University, Evanston, IL 60208, USA.

[5]School of Physical Sciences, University of Chinese Academy of Sciences, Beijing 100049, PR China

[6]Shanghai Collaborative Innovation Center for High Performance Fiber Composites, Donghua University, Shanghai 201620, PR China

[7]Nanjing Institute of Future Energy System, Nanjing 211135, PR China

[*]Corresponding authors: K. Z. (kun.zhang@dhu.edu.cn) and G. L. (gdli@iphy.ac.cn)

Contents

Supplementary Note 1 The failure mechanisms of TEB, BHC-TES and BHC-TEB

Supplementary Note 2 The detailed estimation of electrical output of TET under high temperature difference

Supplementary Note 3 The stress and strain simulation of TET in bending conditions

Supplementary Note 4 The estimation of theoretical voltage and power generation of TET

Supplementary Note 5 The detailed estimation of cooling capacity of TET

Supplementary Note 6 The detailed estimation of maximum cooling capacity of TET

Supplementary Note 7 The detailed estimation of maximum attainable ΔT of TET

Supplementary Note 8 The detailed estimation of coefficient of performance of TET

Supplementary Figure 1 | The manufacturing process of bead-like THC-TES.

Supplementary Figure 2 | The contact angle between TE segment and liquid metal.

Supplementary Figure 3 | The FESEM images and EDS patterns of BST and BTS without and with UHS process.

Supplementary Figure 4 | X-ray diffraction (XRD) patterns of BST w/-UHS **(a)** and BTS w/-UHS **(b)**.

Supplementary Figure 5 | Temperature-dependent electrical thermal conductivity, lattice thermal conductivity **(a)**, power factor (*PF*) **(b)** and *ZT* values **(c)** of BST w/-UHS and BTS w/-UHS.

Supplementary Figure 6 | Brunner-Emmet-Teller (BET) results of BST w/-UHS and BTS w/-UHS.

Supplementary Figure 7 | The diagrams and three-point bending conditions of TEB **(a)**, BHC-TES **(b)**, BHC-TEB **(c)** and THC-TES **(d)** for experimental characterization.

Supplementary Figure 8 | a. The EDS mapping of BTS surface. **b.** The XPS patterns of Te element on sintered PI filaments.

Supplementary Figure 9 | The energy absorption of TEB, BHC-TES, BHC-TEB and THC-TES under three-point bending condition.

Supplementary Figure 10 | The simulation models and operation principles of TEB **(a)**, BHC-TES **(b)**, BHC-TEB **(c)** and THC-TES **(d)**.

Supplementary Figure 11 | The simulated stress at crack tip with different crack growth length of TEB, BHC-TES, BHC-TEB and THC-TES.

Supplementary Figure 12 | Optical images of THC-TES, warp yarn (elastic) and weft yarn using in TET.

Supplementary Figure 13 | The draft plan (top) and denting plan (bottom) of salvage **(a)** and fabric **(b)** using TE yarn. **c.** The lifting plan of TET.

Supplementary Figure 14 | Thermoelectric power generation of TET.

Supplementary Figure 15 | Diagram of the measurement and composition of internal resistance of TET.

Supplementary Figure 16 | The comparison of contact resistivity of flexible TEGs in reported literature[1-9] and this work.

Supplementary Figure 17 | a. The model and operation principle of simplified TET. **b.** The stress distribution of TET. **c.** The stress distribution of TE segments in the TET. The total deformation **(d)** and strain distribution **(e)** of TET. **f.** The strain distribution of TE segments in the TET.

Supplementary Figure 18 | The boundary condition for power generation simulation **(a)** and solid-state cooling simulation **(b)**.

Supplementary Figure 19 | The simulated and measured data of TET in power generation mode and Peltier cooling mode.

Supplementary Figure 20 | The output voltage of TET. The TET was worn on an arm, the ambient temperature is ~8ºC and the surface body temperature is ~32ºC.

Supplementary Figure 21 | The practical application of TET.

Supplementary Figure 22 | The output voltage of TET with human motion.

Supplementary Figure 23 | The calculated cooling capacity (Q_c) and coefficient of performance (*COP*) of TET with 86 pairs **(a)** and 500 pairs **(b)** of TE segments.

Supplementary Table 1 The element composition of p-type BST and n-type BTS TE powders, p-type and n-type TE segment without and with UHS process.

Supplementary Table 2 Details regarding materials' parameters used in the static-structural finite element analysis.

Supplementary Table 3 The estimation parameter of Linearly Fitted ΔT-ΔV curve of TET

Supplementary Table 4 The estimation parameter of output voltage, power and current relationship of TET at high temperature difference

Supplementary Table 5 The calculation of inner resistance of TET

Supplementary Table 6 Details regarding materials' parameters used in the thermal-electric finite element analysis.

Supplementary Table 7 The estimation of theoretical output voltage of TET

Supplementary Table 8 The estimation of theoretical output power of TET

Supplementary Table 9 The calculating of thermal conductivity (κ') of TET

Supplementary Table 10 The calculating parameters of cooling capacity of TET

Supplementary Table 11 The calculating parameter of maximum cooling capacity of TET

Supplementary Table 12 The calculating parameter of maximum attainable ΔT of TET

Supplementary Table 13 The calculating parameter of *COP* of TET

Supplementary Notes

Supplementary Note 1

The failure mechanisms of TEB, BHC-TES and BHC-TEB

Similar to the Line I in Figure 2a, the load-deflection curves of TEB and BHC-TES exhibit linear feature before ultimate fracture (Figure 2b). For TEB, the crack appears and grows fast leading to a typical brittle failure. Hence, the energy is all absorbed by the crack propagation in TEB, thus leading to a huge electrical resistance change to be disconnected (Figure 2c) and a smallest energy absorption of 0.05 mJ (Supplementary Figure 9). For BHC-TES, the crack appears and grows first and then the load was transferred from BTS to PI filaments (similar to the Line II in Figure 2a). Finally, debonding between BTS and PI filaments occurs when the bending load increases further. Therefore, the absorbed energy enhances to 0.66 mJ (Supplementary Figure 9) and the electrical resistance change deceases to 11.4% (Figure 2c). Similar to the Line III in Figure 2a, the energy applied on BHC-TEB is absorbed by PDMS through elastic deformation first and then the crack appears and grows fast leading to ultimate failure of TEB. Afterwards, the energy is reabsorbed by the elastic deformation of PDMS. Although the energy absorption of BHC-TEB enhances to 2.22 mJ (Supplementary Figure 9), the resistance appears a large increase of 108.9% due to lacking of PI filaments (Figure 2c).

Supplementary Note 2

The detailed estimation of electrical output of TET under high temperature difference

The voltage of TET under ΔT of 1.2 K, 2.5 K, 3.8 K, 5.0 K, 6.0 K, 15 K and 25 K are measured as 20.53 mV, 42.03 mV, 61.92 mV, 80.20 mV, 97.29 mV, 237.79 mV and 391.00 mV. Therefore, the ΔV-ΔT curve is linearly fitted to be ΔV=15.835·ΔT+1.804 (R^2=0.9995). Afterwards, giving the value of ΔT=50 K and 80 K, the corresponding voltage is calculated as 793.55 mV and 1268.60 mV.

Since the TET and the external resistance are in series, the fraction that appears across a given resistance in a series circuit is the ratio of the given resistance to the total series resistance according to the voltage-division principle. Therefore, the voltage of the external resistance can be calculate as $U_R = \frac{\Delta V}{R+r}R$. Where, U_R is the voltage of external resistance, ΔV is the open circuit voltage of TET (793.55 mV and 1268.60 mV at ΔT of 50 K and 80 K), R is the external resistance and r is the internal resistance of TET (~30.1 Ω). Hence, $U_R = \frac{\Delta V}{R+r}R$ can be rewritten as $U_R = \frac{793.55}{R+30.1}R$ and $U_R = \frac{1268.60}{R+30.1}R$ when ΔT is 50 K and 80 K. The power of the external resistance can be calculated as $P = \frac{{U_R}^2}{R} = (\frac{\Delta V}{R+r})^2 R$. Therefore, the power can be rewritten as $P = (\frac{793.55}{R+30.1})^2 R$ and $P = (\frac{1268.60}{R+30.1})^2 R$ when ΔT is 50 K and 80 K. The current can be calculated as: $I = \frac{\Delta V}{R+r}$. Hence, the current can be rewritten as $U_R = \frac{793.55}{R+30.1}$ and $U_R = \frac{1268.60}{R+30.1}$ when ΔT is 50 K and 80 K. As a result, the V-I curve, V-P curve and the R-P curve can be obtained by giving a series value of external resistance R.

Supplementary Note 3

The stress and strain simulation of TET in bending conditions

In order to roughly simulate the load and deformation distribution in textile substrate and TE segments in TET during bending process, we simplified the textiles and TE string as block (Supplementary Figure 17).

Supplementary Note 4

The estimation of theoretical voltage and power generation of TET

The theoretical voltage output of the as-prepared TET can be estimated by $|\Delta V| = |N(S_p - S_n)\Delta T|$. The theoretical maximum power output of the as-prepared TET can be estimated by $P_{max} = \frac{\Delta V^2}{4r} = \frac{[N(S_p - S_n)\Delta T]^2}{4r}$. Where, N is the number of thermocouple (86), S_p is the Seebeck coefficient of p-type leg (0.198 mV/K), S_n is the Seebeck coefficient of n-type leg (-0.162 mV/K), r is the internal resistance of TET (30.1 Ω). Therefore, $|\Delta V|$ and P_{max} can be rewritten as: $|\Delta V| = |86 \times (0.198 + 0.162) \times \Delta T| = |30.96\Delta T|$ and $P_{max} = \frac{[N(S_p - S_n)\Delta T]^2}{4r} = \frac{[86\times(0.198+0.162)\times\Delta T]^2}{4\times30.1} = 7.961(\Delta T)^2$. Hence, when ΔT is 1.2 K, 2.5 K, 3.8 K, 5.0 K, 6.0 K, 15 K, 20 K, 25 K, the theoretical ΔV is 33.44 mV, 69.66 mV, 105.88 mV, 139.32 mV, 167.18 mV, 417.96 mV, 557.28 mV and 696.60 mV. The theoretical P_{max} is 9.29 μW, 40.30 μW, 93.12 μW, 161.21 μW, 232.15 μW, 1450.92 μW, 2579.41 μW, 4030.33 μW.

Because of the existence of contact thermal resistance, thermal resistance of the PDMS layer and the power consumption of external circuit, the measured ΔV is 20.53 mV, 42.03 mV, 61.92 mV, 80.20 mV, 97.29 mV, 239.33 mV, 318.50 mV and 397.68 mV, and they are 58.43% of the theoretical ΔV. The measured P_{max} is 3.64 μW, 14.90 μW, 32.06 μW, 53.81 μW, 78.79 μW, 469.40 μW, 814.13 μW, 1269.77 μW, and they are 34.17% of the theoretical P_{max}.

Supplementary Note 5

The detailed estimation of cooling capacity of TET

The heat absorbed from the outside per unit time at the cold side (cooling capacity, Q_c) can be established as: $Q_c = \pi_{TET} T_1 I - \frac{1}{2} I^2 r - k'(T_2 - T_1) = S_{TET} T_1 I - \frac{1}{2} I^2 r - k'(T_2 - T_1) = S_{TET}(T_2 - \Delta T) I - \frac{1}{2} I^2 r - k' \cdot \Delta T$. Where, S_{TET} is the Seebeck coefficient of TET, T_1 is the temperature of cold surface, T_2 is the temperature of hot surface, I is the input current, r is the internal resistance of TET, Q_c is the cooling capacity, k' is the thermal conductivity of TET.

$\kappa' = \frac{N_p A_p}{L_p}\kappa_p + \frac{N_n A_n}{L_n}\kappa_n + \frac{N_{PDMS} A_{PDMS}}{L_{PDMS}}\kappa_{PDMS} + \frac{N_{PI} A_{PI}}{L_{PI}}\kappa_{PI} + \frac{N_{textile} A_{textile}}{L_{textile}}\kappa_{textile}$, N, A, L and κ are the number, area, length and thermal conductivity of each part.

In this work, S_{TET}=0.015835 V/K, T_2=300 K, r=30.1 Ω, N_p=N_n=86, N_{PDMS}=N_{PI}=172, $N_{textile}$=1, A_p=A_n=1 mm^2, A_{PDMS}=3 mm^2, A_{PI}=0.00785 mm^2, $A_{textile}$=15.17 cm^2, L_p=L_n=L_{PDMS}=L_{PI}=$L_{textile}$=5 mm, κ_p=0.62 W/(m·K), κ_n=0.38 W/(m·K), κ_{PDMS}=0.2 W/(m·K), κ_{PI}=0.03 W/(m·K). The calculated κ'=0.06826 W/ K. Therefore, cooling capacity can be rewritten as:

$$Q_c = 0.015835(300 - \Delta T) I - \frac{1}{2} I^2 \times 30.1 - 0.06826 \Delta T$$

(a) ΔT=0.5 K, $Q_c = 4.7426I - 15.05I^2 - 0.03413$

(b) ΔT=1.0 K, $Q_c = 4.7347I - 15.05I^2 - 0.06826$

(c) ΔT=2.0 K, $Q_c = 4.7188I - 15.05I^2 - 0.1365$

(d) ΔT=3.0 K, $Q_c = 4.7030 - 15.05I^2 - 0.2048$

(e) ΔT=5.0 K, $Q_c = 4.6713I - 15.05I^2 - 0.3413$

The cooling capacities of TET with 500 pairs of TE segments are predicted using the same method. As predicted, S_{TET}=0.09206 V/K, T_2=300 K, r=175 Ω, N_p=N_n=500,

N_{PDMS}=N_{PI}=1000, $N_{textile}$=1, A_p=A_n=1 mm^2, A_{PDMS}=3 mm^2, A_{PI}=0.00785 mm^2, $A_{textile}$=88.20 cm^2, L_p=L_n=L_{PDMS}=L_{PI}=$L_{textile}$=5 mm, κ_p=0.62 W/(m·K), κ_n=0.38 W/(m·K), κ_{PDMS}=0.2 W/(m·K), κ_{PI}=0.03 W/(m·K). The calculated κ'=0.3969 W/ K.

Therefore, cooling capacity can be rewritten as:

$$Q_c = 0.09206(300 - \Delta T)I - \frac{1}{2}I^2 \times 175 - 0.3969\Delta T$$

(a) ΔT=0.5 K, $Q_c = 27.5720I - 87.5I^2 - 0.1985$

(b) ΔT=1.0 K, $Q_c = 27.5259I - 87.5I^2 - 0.3969$

(c) ΔT=2.0 K, $Q_c = 27.4339I - 87.5I^2 - 0.7938$

(d) ΔT=3.0 K, $Q_c = 27.3418I - 87.5I^2 - 1.1907$

(e) ΔT=5.0 K, $Q_c = 27.1577I - 87.5I^2 - 1.9845$

All the cooling capacity and input current relationship can be found in Supplementary Figure 23.

Supplementary Note 6

The detailed estimation of maximum cooling capacity of TET

As described in Supplementary Note 5, the cooling capacity can be calculated by equation of $Q_c = S_{TET}T_1I - \frac{1}{2}I^2r - k'(T_2 - T_1)$. Obviously, when the performance of the TET (S_{TET}, r, κ') is constant, the cooling capacity of the TET is related to the current passing through the TET and the temperature difference between the hot side and cold side. That is, for different applied current and temperature difference conditions, the cooling capacity is different. Similarly, if $\frac{dQ_c}{dI} = 0$, the optimal current I can be obtained as $I_q = I_T = \frac{S_{TET}T_1}{r}$. Therefore, the corresponding cooling capacity $Q_c = \frac{1}{2}\frac{{S_{TET}}^2{T_1}^2}{r} - \kappa(T_2 - T_1)$. Further, if it is defined that the TET is in the optimal current working state and the cooling capacity is the maximum when the temperature difference between hot side and cold side is 0, then the cooling capacity Q_{cmax} of the TET can be obtained as $Q_{cmax} = \frac{1}{2}\frac{{S_{TET}}^2{T_1}^2}{r}$.

In this work, S_{TET}=0.015835 V/K, T_1=T_2-ΔT=300-ΔT (T_1 is the temperature of cold side, T_2 is the temperature of hot side, ΔT is temperature difference between hot side and cold side), r=30.1 Ω, Therefore, the limit of cooling capacity can be rewritten as:

$$Q_{cmax} = \frac{1}{2}\frac{{S_{TET}}^2(T_2 - \Delta T)^2}{r} = \frac{1}{2}\frac{0.015835^2(300 - \Delta T)^2}{30.1}$$

Therefore, the maximum cooling capacity Q_{cmax} is 0.374 W, 0.372 W, 0.370 W, 0.367 W and 0.362 W when ΔT is 0.5 K, 1.0 K, 2.0 K, 3.0 K and 5.0 K.

Supplementary Note 7

The detailed estimation of maximum attainable *ΔT* of TET

The maximum attainable *ΔT* is related to the cooling capacity of the TET and the external thermal load. Using the heat balance equation of the cold side of TET $Q_c = S_{TET}T_1I - \frac{1}{2}I^2r - k'(T_2 - T_1) = S_{TET}T_1I - \frac{1}{2}I^2r - k' \cdot \Delta T$ (Supplementary Note 5), it can be obtained that $\Delta T = \frac{S_{TET}T_1I - \frac{1}{2}I^2r - Q_c}{k'}$. For the condition of no external thermal load (Q_c=0), if $\frac{d(\Delta T)}{dI} = 0$, the optimal current *I* can be obtained as $I_T = \frac{S_{TET}T_1}{r}$. When the TET works at this optimal current, the maximum temperature difference ΔT_{max} can be calculated according the equation: $\Delta T_{max} = \frac{1}{2}ZT_1{}^2$. Because $\Delta T=T_2-T_1$ (T_1 is the temperature of cold side, T_2 is the temperature of hot side, ΔT is temperature difference between hot side and cold side), $\Delta T_{max} = T_2 - T_{1min} = \frac{1}{2}ZT_1{}^2$. Hence, $T_{1min} = \frac{\sqrt{1+2zT_2}-1}{Z}$, where $Z = \frac{S_{TET}{}^2}{r\kappa'}$. In this work, S_{TET}=0.015835 V/K, T_2=300 K, r=30.1 Ω, κ'=0.06826 W/ K (Supplementary Note 5 and Supplementary Table 9). Therefore, T_{1min} and ΔT_{max} are calculated to be 294.7 K and 5.3 K.

Supplementary Note 8

The detailed estimation of coefficient of performance of TET

The coefficient of performance (*COP*) of the as-prepared TET is defined as: $COP = \frac{Q_C}{P}$, where, Q_c is the cooling capacity of TET (Supplementary Note 5 and Supplementary Table 10), P is input power. The applied voltage V across the TET should be equal to the voltage drop across the TET (V_R=Ir) plus the voltage drop required to oppose the Seebeck voltage V_S=S_{TET}(T_2-T_1), that is, $V = V_R + V_S = Ir + S_{TET}(T_2 - T_1)$. Therefore, the input power P can be obtained as $P = IV = I^2r + S_{TET}(T_2 - T_1)I = I^2r + S_{TET}\Delta TI$. Then, the *COP* can be calculated as: $COP = \frac{Q_C}{P} = \frac{S_{TET}T_1I - \frac{1}{2}I^2r - k'\cdot\Delta T}{I^2r + S_{TET}\Delta TI}$. In this work, S_{TET}=0.015835 V/K, T_1=T_2-ΔT=300-ΔT (T_1 is the temperature of cold side, T_2 is the temperature of hot side, ΔT is temperature difference between hot side and cold side), r=30.1 Ω, κ'=0.06826 W/K (Supplementary Note 5 and Supplementary Table 9). Therefore, *COP* can be rewritten as:

$$COP = \frac{0.015835(300 - \Delta T)I - \frac{1}{2}I^2 \times 30.1 - 0.06826\Delta T}{30.1I^2 + 0.015835\Delta TI}$$

(a) ΔT=0.5 K, $COP = \frac{4.7426I - 15.05I^2 - 0.03413}{30.1I^2 + 0.007918I}$

(b) ΔT=1.0 K, $COP = \frac{4.7347I - 15.05I^2 - 0.06826}{30.1I^2 + 0.01584I}$

(c) ΔT=2.0 K, $COP = \frac{4.7188I - 15.05I^2 - 0.1365}{30.1I^2 + 0.03167I}$

(d) ΔT=3.0 K, $COP = \frac{4.7030I - 15.05I^2 - 0.2048}{30.1I^2 + 0.04751I}$

(e) ΔT=5.0 K, $COP = \frac{4.6713I - 15.05I^2 - 0.3413}{30.1I^2 + 0.07918I}$

The *COP* of TET with 500 pairs of TE segments are predicted using the same method. As predicted, S_{TET}=0.09206 V/K, T_1=T_2-ΔT=300-ΔT (T_1 is the temperature of

cold side, T_2 is the temperature of hot side, ΔT is temperature difference between hot side and cold side), r=175 Ω, κ'=0.3969 W/ K (Supplementary Note 5 and Supplementary Table 9). Therefore, *COP* can be rewritten as:

$$COP = \frac{0.09206(300 - \Delta T)I - \frac{1}{2}I^2 \times 175 - 0.3969\Delta T}{175I^2 + 0.09206\Delta TI}$$

(a) ΔT=0.5 K, $COP = \frac{27.5720I - 87.5I^2 - 0.1985}{175I^2 + 0.04603I}$

(b) ΔT=1.0 K, $COP = \frac{27.5259I - 87.5I^2 - 0.3969}{175I^2 + 0.9206I}$

(c) ΔT=2.0 K, $COP = \frac{27.4339I - 87.5I^2 - 0.7938}{175I^2 + 0.18412I}$

(d) ΔT=3.0 K, $COP = \frac{27.3418I - 87.5I^2 - 1.1907}{175I^2 + 0.27618I}$

(e) ΔT=5.0 K, $COP = \frac{27.1577I - 87.5I^2 - 1.9845}{175I^{2+0.4603I}}$

All the *COP* and input current relationship can be found in Supplementary Figure 23.

Supplementary Figures

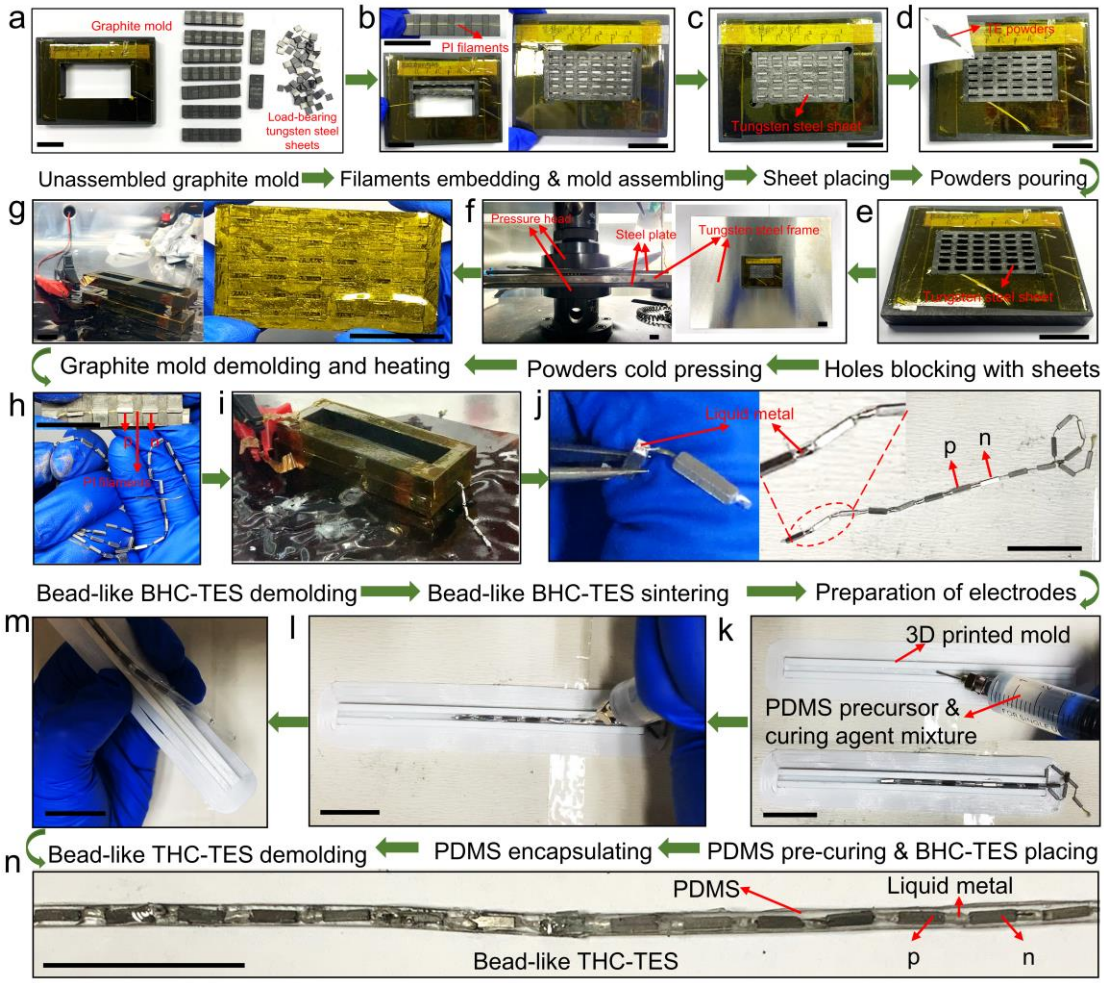

Supplementary Figure 1 | The manufacturing process of bead-like THC-TES. **a.** The mold used to produce bead-like THC-TES. **b.** Placed the cleaned PI filaments in the middle of each graphite mold in a complete sequence (the diameter of PI filaments is ~0.1 mm). **c.** Put the tungsten steel sheets (5×4.5 mm^2) into the holes (1×5 mm^2) between each graphite mold on one side. **d.** Put the p-type and n-type powders into the holes between each graphite mold on the other side alternatively. **e.** Blocked the holes containing TE powders with tungsten steel sheets (5×5.5 mm^2). **f.** Placed the whole graphite mold achieved by **(e)** in a tungsten steel frame and applied a pressure of 200

MPa for 1 h to mold the TE powders. **g.** Demolded the graphite mold from the tungsten steel frame and heated it through two pieces of carbon paper (TORAY, TGP-H-060, 62 mm in length, 12 mm in width and 0.19 mm in thickness) under a current of 4.5 A for 30 min under Ar atmosphere (supplied power is ~61 W). **h.** Demolded the BHC-TES from the graphite mold. **i.** Sintered the BHC-TES through the two pieces of carbon paper under a current of 5.5 A for 10 s under Ar atmosphere (supplied power is ~91 W). **j.** Brushed liquid metal onto the surface of TE segment with a cotton swab to pre-wet the connecting surface. Injected liquid metal on the PI filaments to connect p-type and n-type TE segment. Note: the length of inter-electrode made by liquid metal is 2 mm. **k.** Injected the mixture of PDMS precursor and curing agent (ratio of precursor and curing agent is 10:1) into a 3D printed mold (2 mm in width and 2 mm in depth) for 0.5 mm-thick and pre-cured it at 55ºC for 30 min. Subsequently, placed the BHC-TES coated with liquid metal (the sample obtained in **(j)**) on the pre-cured PDMS layer. **l.** Injected the mixture of PDMS precursor and curing agent into the mold again until full fill the mold. **m.** Cured and demolded the bead-like THC-TES **(n)**. Scale bar: 20 mm.

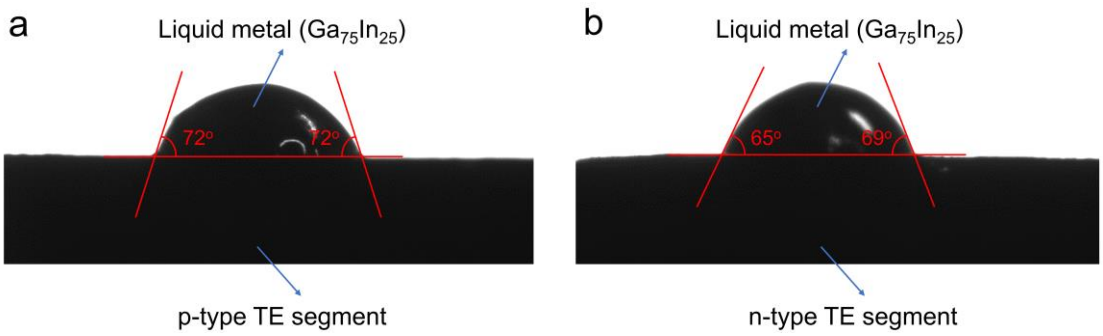

Supplementary Figure 2 | The contact angle between TE segment and liquid metal.

a. p-type TE segment. **b.** n-type TE segment.

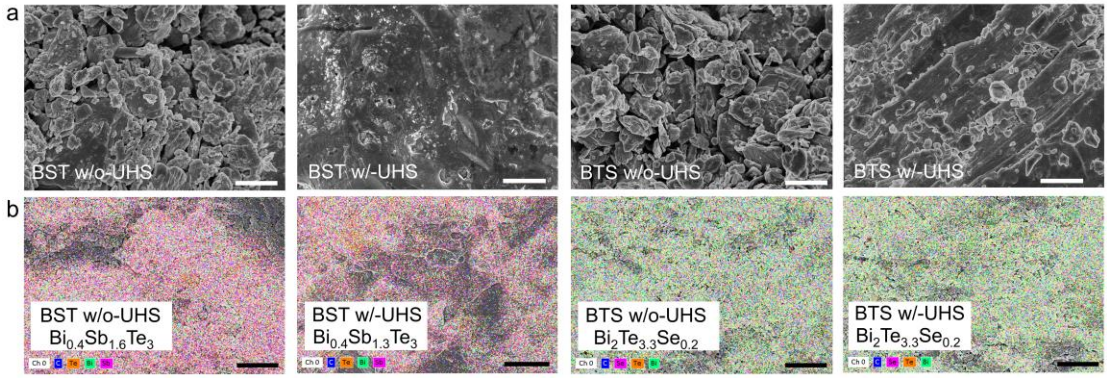

Supplementary Figure 3 | The FESEM images and EDS patterns of BST and BTS without and with UHS process. **a.** The FESEM images of the surface of BST w/o-UHS, BST w/-UHS, BTS w/o-UHS and BTS w/-UHS. Scale bar: 2 μm. **b.** The EDS patterns of the surface of BST w/o-UHS, BST w/-UHS, BTS w/o-UHS and BTS w/-UHS. Scale bar: 10 μm.

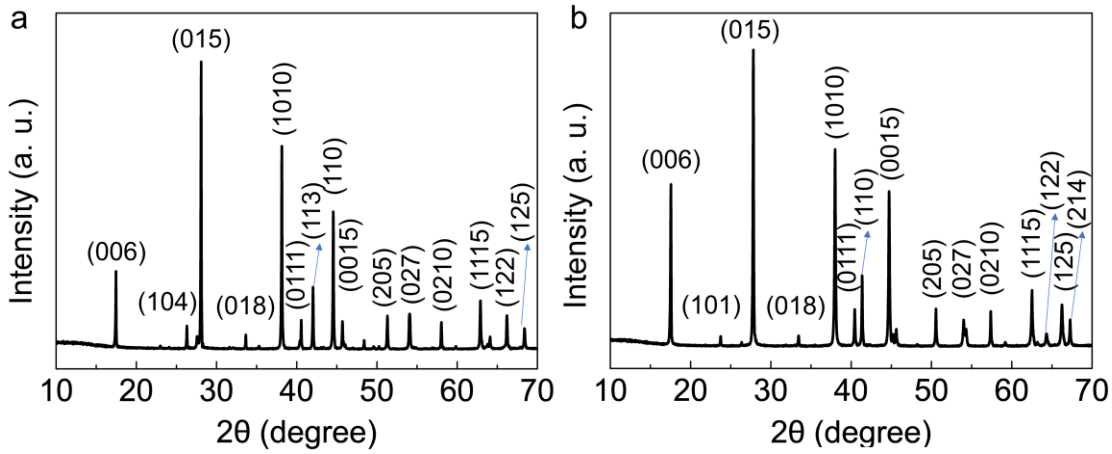

Supplementary Figure 4 | X-ray diffraction (XRD) patterns of BST w/-UHS **(a)** and BTS w/-UHS **(b)**.

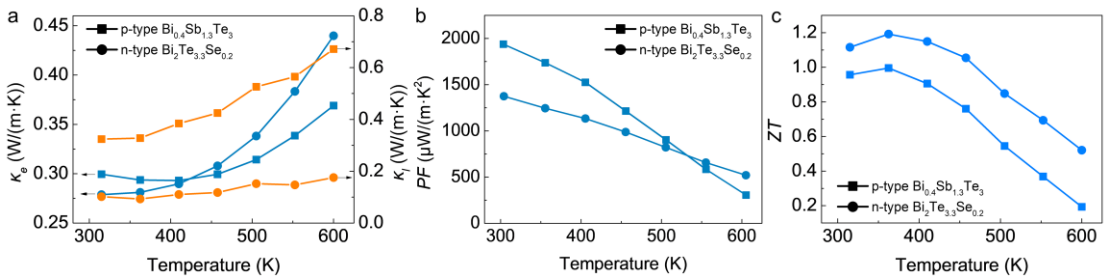

Supplementary Figure 5 | Temperature-dependent electrical thermal conductivity, lattice thermal conductivity **(a)**, power factor (*PF*) **(b)** and *ZT* values **(c)** of BST w/-UHS and BTS w/-UHS.

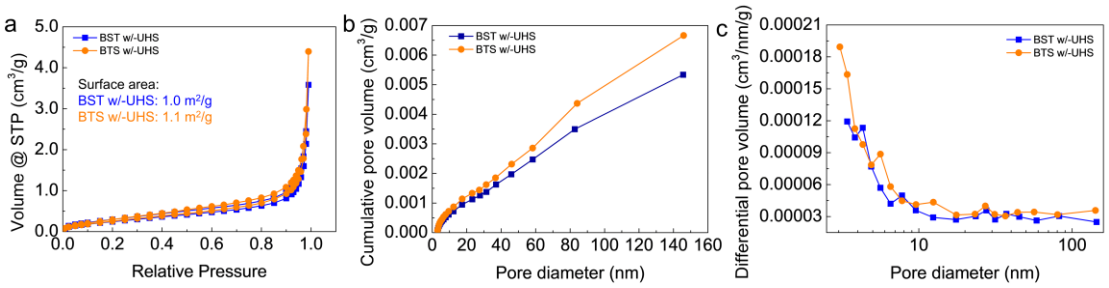

Supplementary Figure 6 | Brunner-Emmet-Teller (BET) results of BST w/-UHS and BTS w/-UHS. Isotherms **(a)**, cumulative **(b)**, and differential pore volume distributions **(c)** for BST w/-UHS and BTS w/-UHS.

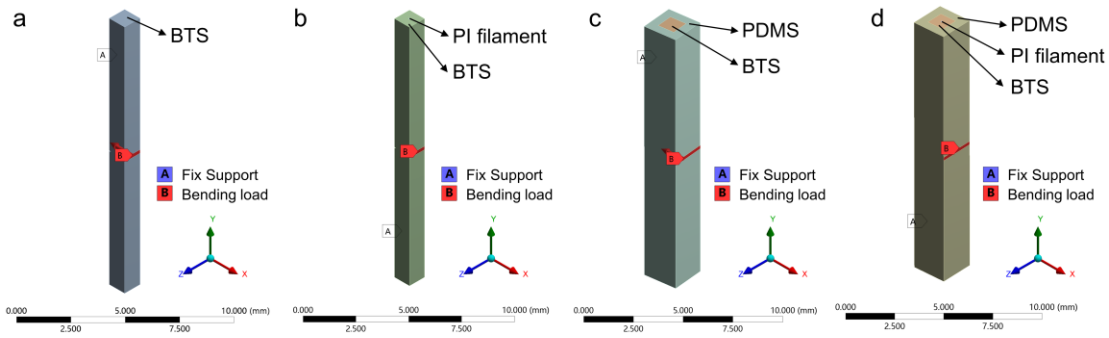

Supplementary Figure 7 | The diagrams and three-point bending conditions of TEB **(a)**, BHC-TES **(b)**, BHC-TEB **(c)** and THC-TES **(d)** for experimental characterization.

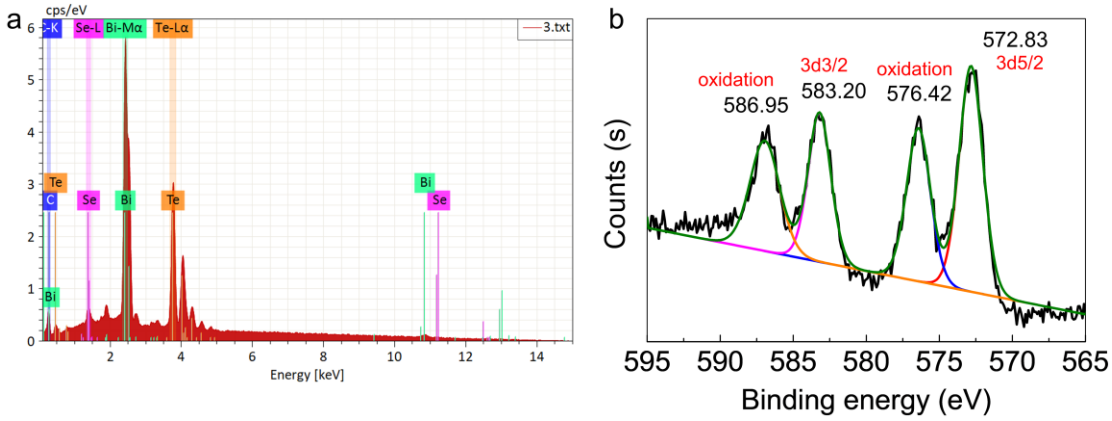

Supplementary Figure 8 | a. The EDS mapping of BTS surface. **b.** The XPS patterns of Te element on sintered PI filaments.

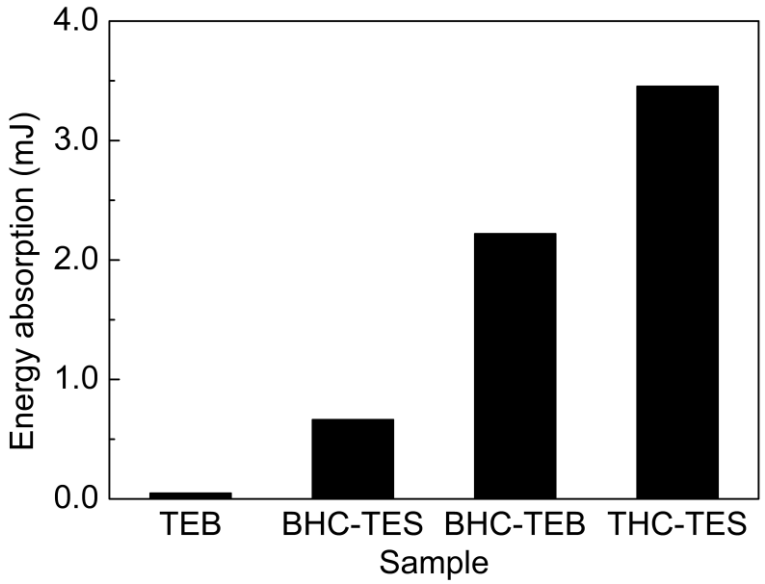

Supplementary Figure 9 | The energy absorption of TEB, BHC-TES, BHC-TEB and THC-TES under three-point bending condition. The energy absorption is calculated from the area in Figure 2b.

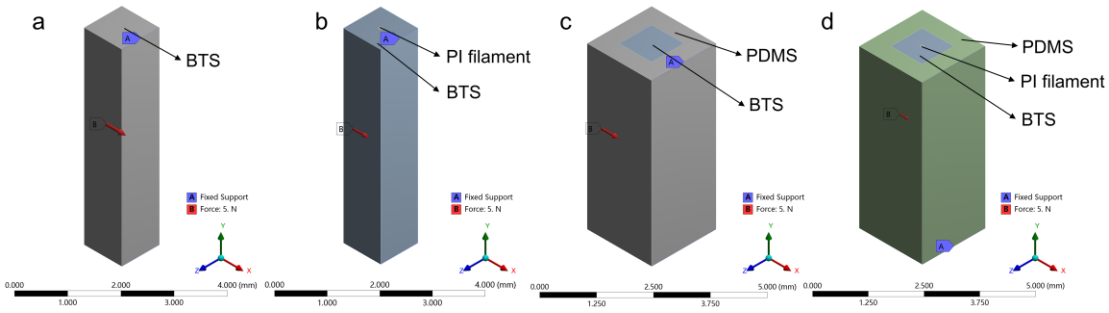

Supplementary Figure 10 | The simulation models and operation principles of TEB **(a)**, BHC-TES **(b)**, BHC-TEB **(c)** and THC-TES **(d)**.

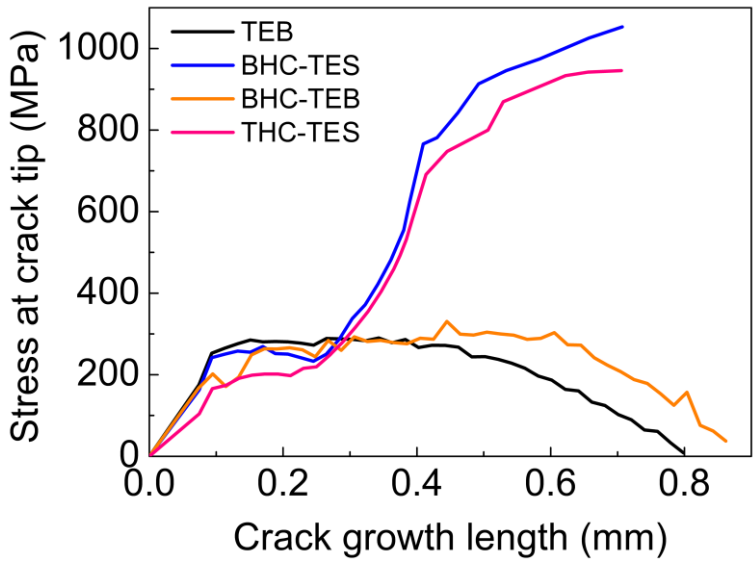

Supplementary Figure 11 | The simulated stress at crack tip with different crack growth length of TEB, BHC-TES, BHC-TEB and THC-TES.

Supplementary Figure 12 | Optical images of THC-TES, warp yarn (elastic) and weft yarn using in TET.

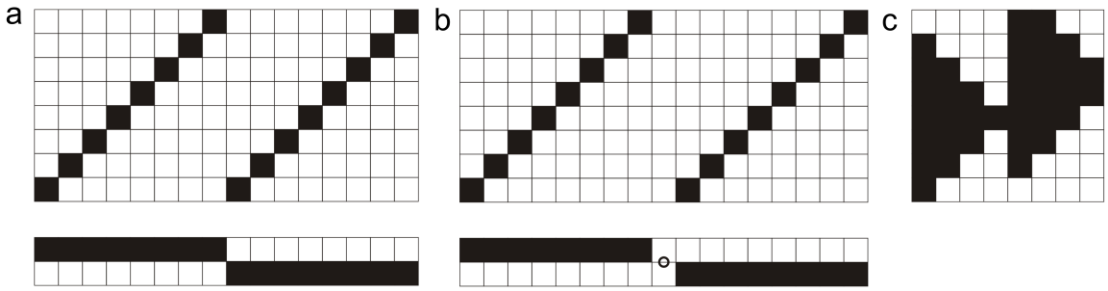

Supplementary Figure 13 | The draft plan (top) and denting plan (bottom) of salvage **(a)** and fabric **(b)** using TE yarn. **c.** The lifting plan of TET.

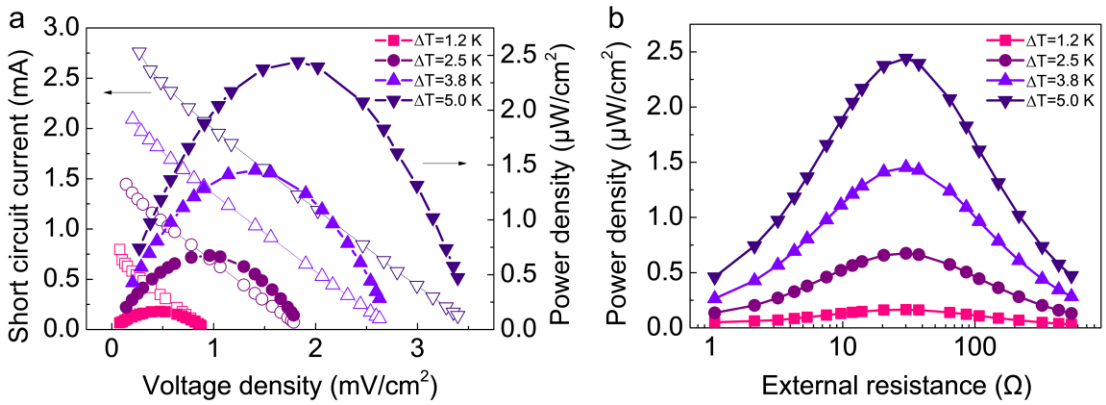

Supplementary Figure 14 | Thermoelectric power generation of TET. **a.** Short circuit current and power density as a function of voltage density at different ΔT. **b.** Output power density of TET as a function of external resistance at different ΔT.

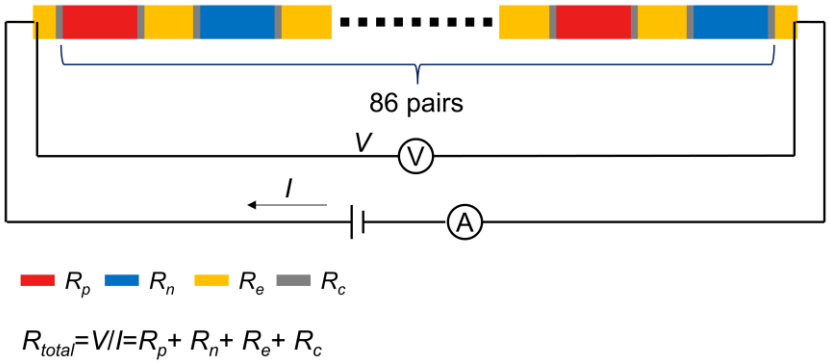

Supplementary Figure 15 | Diagram of the measurement and composition of internal resistance of TET.

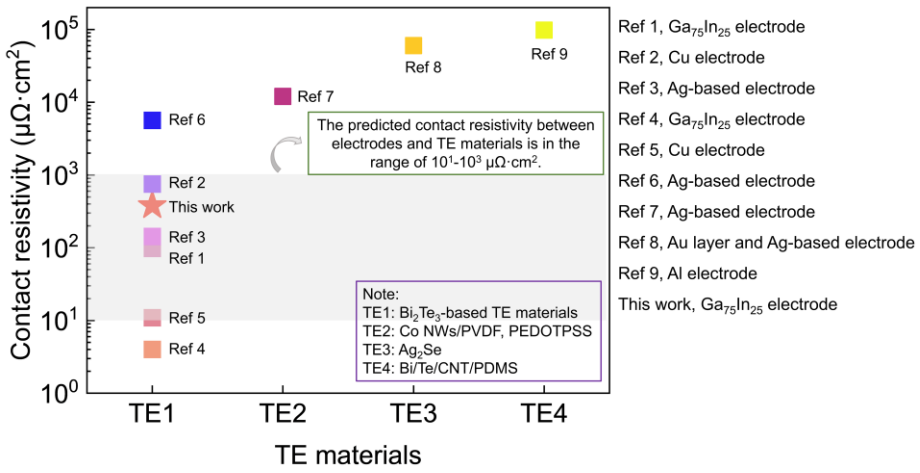

Supplementary Figure 16 | The comparison of contact resistivity of flexible TEGs in reported literature[1-9] and this work.

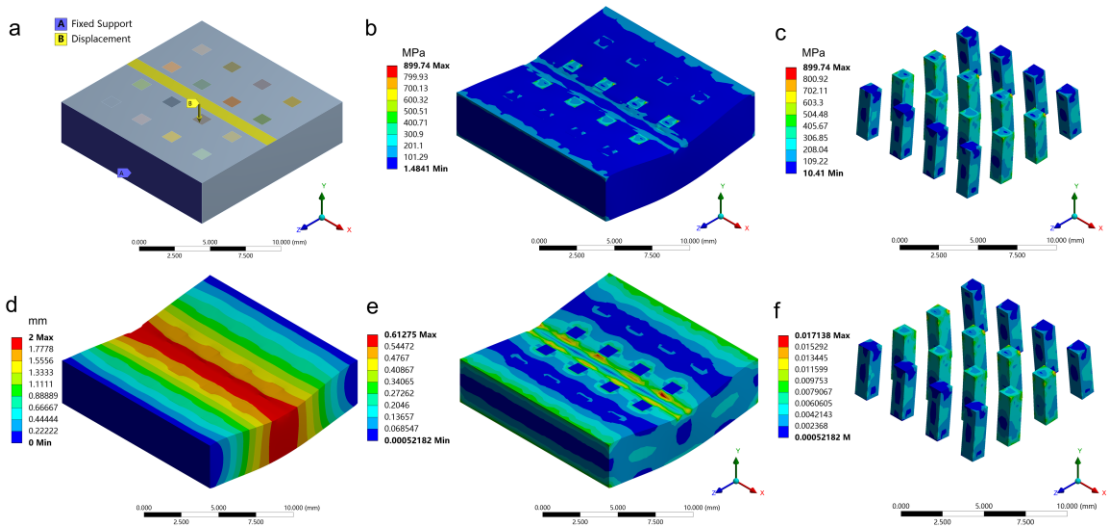

Supplementary Figure 17 | a. The model and operation principle of simplified TET. **b.** The stress distribution of TET. **c.** The stress distribution of TE segments in the TET. The total deformation **(d)** and strain distribution **(e)** of TET. **f.** The strain distribution of TE segments in the TET.

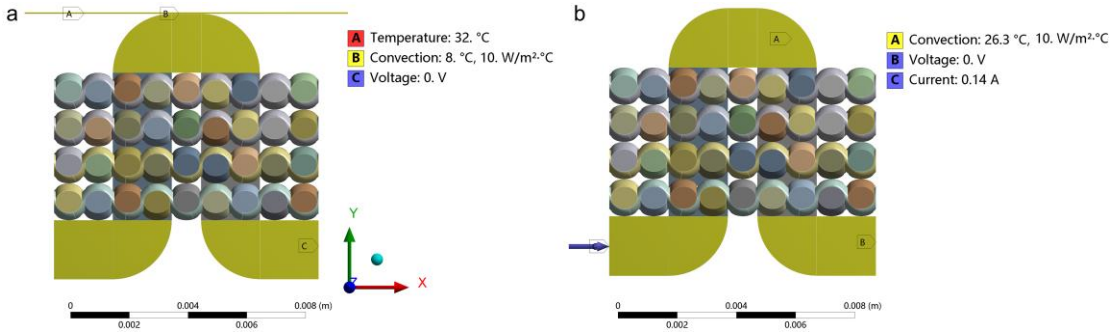

Supplementary Figure 18 | The boundary condition for power generation simulation **(a)** and solid-state cooling simulation **(b)**.

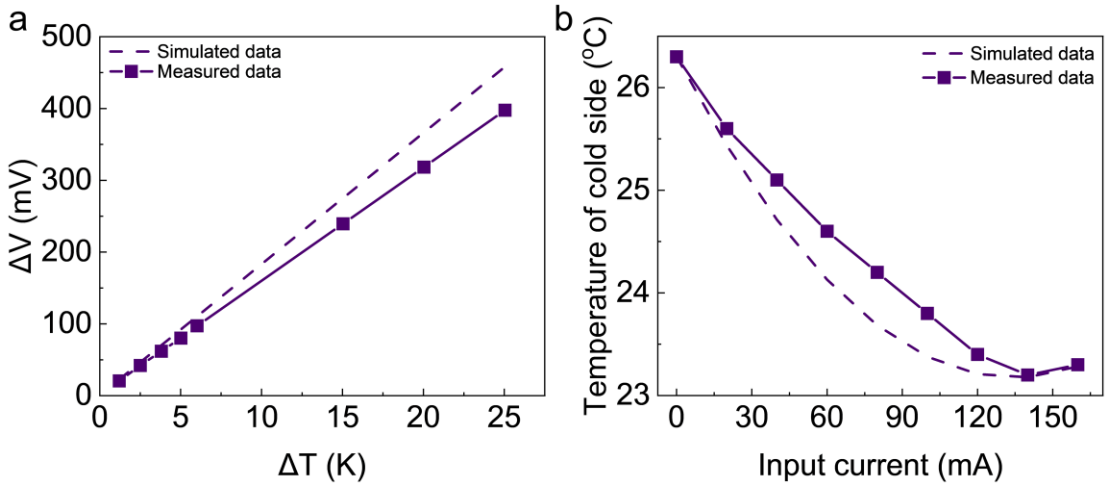

Supplementary Figure 19 | The simulated and measured data of TET in power generation mode and Peltier cooling mode. **a.** The output voltage of TET with altered applied temperature difference. **b.** The temperature decrease of TET with altered input current.

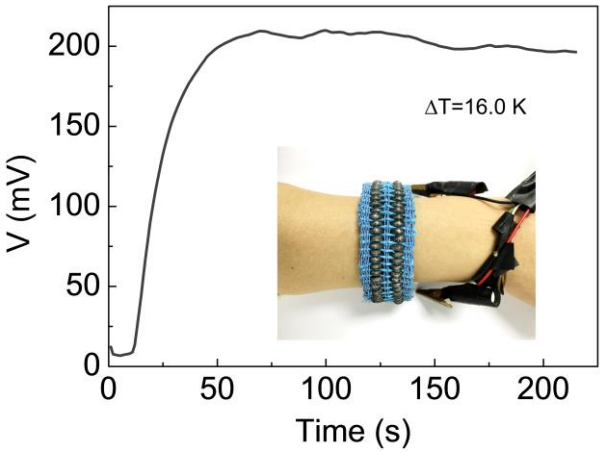

Supplementary Figure 20 | The output voltage of TET. The TET was worn on an arm, the ambient temperature is ~8ºC and the surface body temperature is ~32ºC.

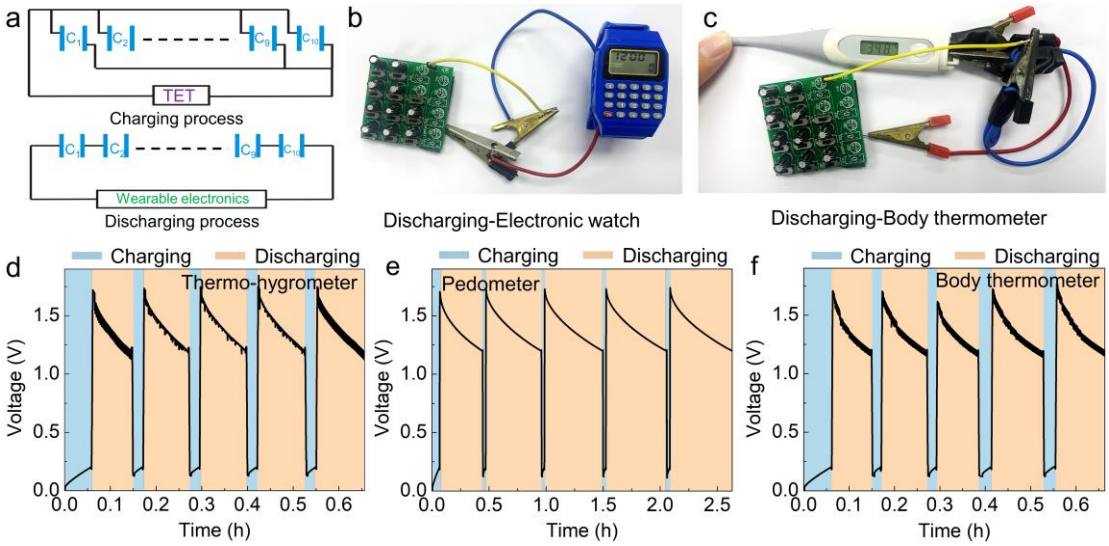

Supplementary Figure 21 | The practical application of TET. **a.** Circuit diagrams of charging supercapacitors in in-parallel mode through TET (top) and powering wearable electronics by supercapacitors switched to in-series mode (bottom). Optical images of powering electronic watch **(b)** and body thermometer **(c)** by charged supercapacitors. Voltage of supercapacitors which are charged by TET and discharged by thermo-hygrometer **(d)**, pedometer **(e)** and body thermometer **(f)**.

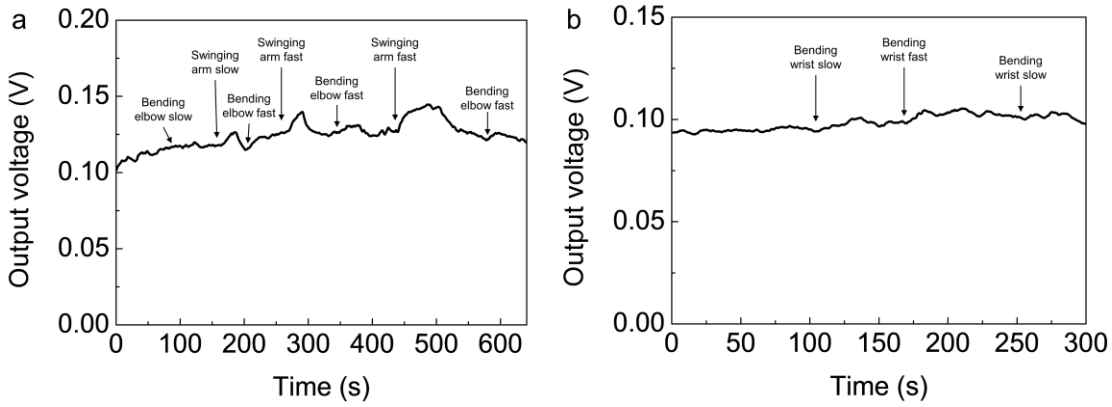

Supplementary Figure 22 | The output voltage of TET with human motion. **a.** TET wearing on elbow. **b.** TET wearing on wrist ($T_{ambient}$: ~20ºC).

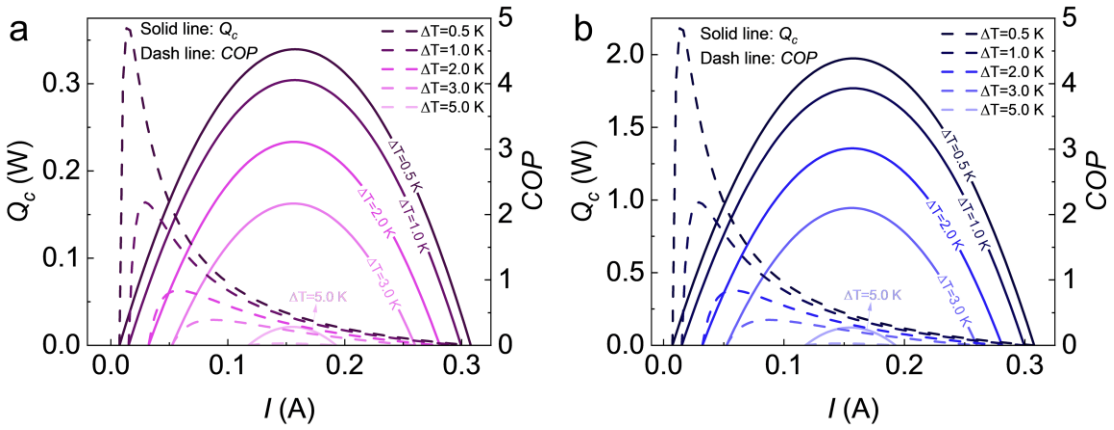

Supplementary Figure 23 | The calculated cooling capacity (Q_c) and coefficient of performance (COP) of TET with 86 pairs **(a)** and 500 pairs **(b)** of TE segments.

Supplementary Tables

Supplementary Table 1 The element composition of p-type BST and n-type BTS TE powders, p-type and n-type TE segment without and with UHS process.

	Bi (at%)	Te (at%)	Sb (at%)	Se (at%)
BST TE powders	6.25	68.64	25.11	/
BST w/o-UHS	7.62	59.72	32.66	/
BST w/-UHS	7.87	63.96	28.17	/
BTS TE powders	30.99	66.51	/	2.50
BTS w/o-UHS	36.83	59.97	/	3.20
BTS w/-UHS	36.74	60.28	/	2.98

Supplementary Table 2 Details regarding materials' parameters used in the static-structural finite element analysis.

Materials	Young's modulus (GPa)	Poisson's ratio	Bulk modulus (GPa)	Shear modulus (GPa)	Density (g/cm^3)
TE bulk	0.898	0.25	0.599	0.359	5.70
PI filaments	21.96	0.4	36.60	7.84	1.43
PDMS	3×10^{-3}	0.3	2.5×10^{-3}	1.15×10^{-3}	0.92

Supplementary Table 3 The estimation parameter of Linearly Fitted *ΔT*-*ΔV* curve of TET

ΔT/K	*ΔV*/mV	Note	Linearly Fitted *ΔT*-*ΔV* curve
1.2	20.53	Measured	
2.5	42.03	Measured	
3.8	61.92	Measured	
5.0	80.20	Measured	ΔV=15.835·ΔT+1.809 (R^2=0.9995)
6.0	97.29	Measured	
15	239.33	Fitted	
25	397.68	Fitted	

Note: *ΔT* is temperature difference, *ΔV* is output voltage.

Supplementary Table 4 The estimation parameter of output voltage, power and current relationship of TET at high temperature difference

ΔT/K	ΔV/mV	r/Ω	Equation	Circuit diagram
50	793.55	30.1	$P = (\frac{\Delta V}{R+r})^2 R$	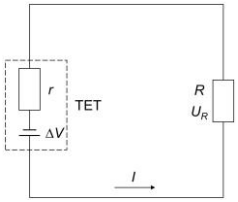
80	1268.60	30.1	$I = \frac{\Delta V}{R+r}$	

Note: ΔT is temperature difference, ΔV is output voltage, r is the internal resistance of TET, R is the external resistance, U_R is the voltage of external resistance.

Supplementary Table 5 The calculation of inner resistance of TET

	σ/S/cm	A/cm^2	L/cm	N	Equation	R/Ω
p-type segment	493	0.01	0.5	86		8.722
n-type segment	524	0.01	0.5	86	$R = \frac{NL}{\sigma A}$	8.206
$Ga_{75}In_{25}$	34600	0.01	0.2	173		0.1
Contact resistance	/	/	/	344	/	13.07
Total resistance	/	/	/	/	/	30.1

Note: σ, A, L, N and R are the electrical conductivity, cross-section area, length, number and resistance of each composition.

Contact resistance=(Total resistance)-(resistance of p-type segments)-(resistance of n-type segments)-(resistance of $Ga_{75}In_{25}$).

Single contact resistance=(Contact resistance)/N=13.07/344=38 mΩ.

Contact resistivity=(Contact resistance)×A=380 μΩ·cm^2.

Supplementary Table 6 Details regarding materials' parameters used in the thermal-electric finite element analysis.

Materials	κ (W/m·K)	ρ (Ω·m)	S (μV/K)
PDMS	0.2	/	/
PI filament	0.03	/	/
Liquid metal	26.43	2.89×10^{-7}	/
P-type leg	0.62	2.03×10^{-5}	198
N-type leg	0.38	1.91×10^{-5}	-162
Warp yarn	0.263	/	/
Weft yarn	0.04	/	/

Supplementary Table 7 The estimation of theoretical output voltage of TET

ΔT /K	S_p /mV/K	S_n /mV/K	N	Equation	ΔT_{th} /mV	ΔT_m /mV	ΔT_m /ΔT_{th}
1.2	0.198	-0.126	86	$\lvert\Delta V\rvert = \lvert N(S_p - S_n)\Delta T\rvert$	33.44	20.53	0.6140
2.5	0.198	-0.126	86		69.66	42.03	0.6034
3.8	0.198	-0.126	86		105.88	61.92	0.5848
5	0.198	-0.126	86		139.32	80.2	0.5757
6	0.198	-0.126	86		167.18	97.29	0.5819
15	0.198	-0.126	86		417.96	239.33	0.5726
20	0.198	-0.126	86		557.28	318.5	0.5715
25	0.198	-0.126	86		696.60	397.68	0.5709

Note: ΔT_{th} and ΔT_m represent the theoretical and measured output voltage of TET.

Supplementary Table 8 The estimation of theoretical output power of TET

ΔT /K	S_p /mV/K	S_n /mV/K	N	r/Ω	Equation	$P_{max\text{-}th}$ /μW	$P_{max\text{-}m}$ /μW	$P_{max\text{-}m}$ /$P_{max\text{-}th}$
1.2	0.198	-0.126	86	30.1		9.29	3.64	0.3920
2.5	0.198	-0.126	86	30.1		40.30	14.9	0.370
3.8	0.198	-0.126	86	30.1		93.12	32.06	0.3443
5	0.198	-0.126	86	30.1	$P_{max} = \frac{\Delta V^2}{4r}$	161.21	53.81	0.3338
6	0.198	-0.126	86	30.1	$= \frac{[N(S_p - S_n)\Delta T}{4r}$	232.15	78.79	0.3394
15	0.198	-0.126	86	30.1		1450.92	469.4	0.3235
20	0.198	-0.126	86	30.1		2579.41	814.13	0.3156
25	0.198	-0.126	86	30.1		4030.33	1269.77	0.3151

Note: $P_{max\text{-}th}$ and $P_{max\text{-}m}$ represent the theoretical and measured output power of TET.

Supplementary Table 9 The calculating of thermal conductivity (*κ*') of TET

86 pairs of TET	A/m^2	L/m	κ/W/m K	N	κ'/W/K
p-type segment	1×10^{-6}	0.005	0.62	86	0.010664
n-type segment	1×10^{-6}	0.005	0.38	86	0.006536
PDMS layer	3×10^{-6}	0.005	0.2	172	0.02064
PI filaments	7.85×10^{-8}	0.005	0.03	172	8.1E-05
Textile substrate	1.517×10^{-3}	0.005	0.1	1	0.03034
κ' (total)					0.06826
500 pairs of TET	A/m^2	L/m	κ/W/m K	N	κ'/W/K
p-type segment	1×10^{-6}	0.005	0.62	500	0.062
n-type segment	1×10^{-6}	0.005	0.38	500	0.038
PDMS layer	3×10^{-6}	0.005	0.2	1000	0.12
PI filaments	7.85×10^{-8}	0.005	0.03	1000	0.000471
Textile substrate	8.82×10^{-3}	0.005	0.1	1	0.1764
κ' (total)					0.3969

Note: N, A, L and κ are the number, area, length and thermal conductivity of each part. κ' is the thermal conductivity.

Supplementary Table 10 The calculating parameters of cooling capacity of TET

N	S_{TET}/V/K	T_2/K	ΔT/K	r	κ'	Equation
86	0.015835	300	0.5	30.1	0.06826	
86	0.015835	300	1	30.1	0.06826	
86	0.015835	300	2	30.1	0.06826	
86	0.015835	300	3	30.1	0.06826	
86	0.015835	300	5	30.1	0.06826	$Q_c = S_{TET}(T_2 - \Delta T) - \frac{1}{2}I^2 r$
500	0.09206	300	0.5	175	0.3969	$- k' \cdot \Delta T$
500	0.09206	300	1	175	0.3969	
500	0.09206	300	2	175	0.3969	
500	0.09206	300	3	175	0.3969	
500	0.09206	300	5	175	0.3969	

Supplementary Table 11 The calculating parameter of maximum cooling capacity of TET

S_{TET}/V/K	T_2/ K	$T_1=T_2-\Delta T$	r/Ω	ΔT	$Q_{cmax}=\frac{1}{2}\frac{{S_{TET}}^2{T_1}^2}{r}$
				0.5	0.374
				1	0.372
0.015835	300	300-ΔT	30.1	2	0.370
				3	0.367
				5	0.362

Supplementary Table 12 The calculating parameter of maximum attainable ΔT of TET

S_{TET}/V/K	r/Ω	κ'/W/K	T_2/K	$Z = \frac{S_{TET}^2}{r\kappa'}$	$T_{1min} = \frac{\sqrt{1+2zT_2}-1}{Z}$	ΔT_{max}= T_2-T_{1min}
0.015835	30.1	0.06826	300	1.2204×10^{-4}	294.7	5.3

Supplementary Table 13 The calculating parameter of *COP* of TET

S_{TET}/V/K	T_2/ K	$T_1=T_2-\Delta T$	r/Ω	κ'	ΔT	Equation
0.015835	300	300-ΔT	30.1	0.06826	0.5 1 2 3 5	$\frac{S_{TET}T_1I-\frac{1}{2}I^2r-k'\cdot\Delta}{I^2r+S_{TET}\Delta TI}$

References

1. M. Zadan, M. H. Malakooti and C. Majidi, *ACS Appl. Mater. Interfaces*, 2020, **12**, 17921-17928.
2. Y. Yang, H. Hu, Z. Chen, Z. Wang, L. Jiang, G. Lu, X. Li, R. Chen, J. Jin, H. Kang, H. Chen, S. Lin, S. Xiao, H. Zhao, R. Xiong, J. Shi, Q. Zhou, S. Xu and Y. Chen, *Nano Lett.*, 2020, **20**, 4445-4453.
3. Y. Ekubaru, T. Sugahara, K. Ibano, A. Suetake, M. Tsurumoto, N. Kagami and K. Suganuma, *Adv. Mater. Technol.*, 2020, **5**, 1901128.
4. F. Suarez, D. P. Parekh, C. Ladd, D. Vashaee, M. D. Dickey and M. C. Öztürk, *Appl. Energy*, 2017, **202**, 736-745.
5. S. J. Kim, H. E. Lee, H. Choi, Y. Kim, J. H. We, J. S. Shin, K. J. Lee and B. J. Cho, *ACS Nano*, 2016, **10**, 10851-10857.
6. T. Varghese, C. Dun, N. Kempf, M. Saeidi-Javash, C. Karthik, J. Richardson, C. Hollar, D. Estrada and Y. Zhang, *Adv. Funct. Mater.*, 2020, **30**, 1905796.
7. Y. Chen, M. He, J. Tang, G. C. Bazan and Z. Liang, *Adv. Electron. Mater.*, 2018, **4**, 1800200.
8. C. Jiang, Y. Ding, K. Cai, L. Tong, Y. Lu, W. Zhao and P. Wei, *ACS Appl. Mater. Interfaces*, 2020, **12**, 9646-9655.
9. K. K. Jung, Y. Jung, C. J. Choi, J. M. Lee and J. S. Ko, *Curr. Appl. Phys.*, 2016, **16**, 1442-1448.